https://doi.org/10.5194/egusphere-2026-577
Preprint. Discussion started: 20 February 2026

Rating Surfaces for Quantifying Compound Flooding at Points of Interest

Mark Wang[1], Paola Passalacqua[2,1], Hamed Moftakhari[3], and Bailley Hardage[1]

[1]Fariborz Maseeh Department of Civil, Architectural, and Environmental Engineering, Center for Water and the Environment, University of Texas at Austin, Austin, USA
[2]Institute of Environmental Engineering, Department of Civil, Environmental and Geomatic Engineering, ETH Zürich, Zürich, CH
[3]Department of Civil, Construction and Environmental Engineering, Center for Complex Hydrosystems Research, University of Alabama, Tuscaloosa, USA

Correspondence: Paola Passalacqua (ppassalacqua@ethz.ch)

Abstract. Compound flooding in low-relief coastal regions arises from interactions among coastal water levels, river discharge, and precipitation. Capturing these interactions typically requires coupled hydrodynamic models, which can be computationally intensive, limiting their use in high-resolution or large-ensemble analyses. In this study, we introduce rating surfaces: two-dimensional plots that provide contours of compound flood depth at points of interest given pairs of potentially interacting flood drivers. Using Southeast Texas as a testbed, we generate synthetic inundation scenarios with both efficient terrain-based models (c-HAND, GeoFlood, and Fill-Spill-Merge) and the reduced-physics hydrodynamic model SFINCS. Sampling these scenarios at points of interest yields rating surfaces that characterize how precipitation, discharge, and coastal water level jointly influence maximum compound flood depth. Across locations, simplified and hydrodynamic models produce similar depth patterns, but SFINCS captures finer-scale nonlinearities. The two approaches provide comparable depth estimates, and their prediction envelope typically includes the observed high-water marks. Rating surfaces provide an efficient tool for evaluating compound flooding in settings where computational constraints challenge traditional hydrodynamic modeling, offering a framework for scenario assessment and communication of compound flood hazards at points of interest.

1 Introduction

Flooding is the most frequent and widespread natural disaster; it has affected over 2 billion people globally from 1998 to 2017 (Wallemacq et al., 2018) and it costs the United States over $180 billion annually (U.S. Congress, 2024). Over 50% of the U.S. population now lives in coastal watersheds (Crossett et al., 2013), and the global coastal population is projected to exceed 1 billion by 2060 (Neumann et al., 2015; Reimann et al., 2023). Tropical cyclones threaten coastal areas (Dullaart et al., 2021), causing damages over $1.425 trillion in the United States from 1980 to 2024 with an average cost of $22.3 billion per event (Smith, 2024). Tropical cyclones have caused severe and deadly coastal flooding in recent years, with examples

https://doi.org/10.5194/egusphere-2026-577
Preprint. Discussion started: 20 February 2026

including Hurricane Harvey (2017), Tropical Storm Imelda (2019), Hurricanes Isaias, Laura (2020), Ida (2021), Helene, and Milton (2024). As coastal populations grow and face increasing exposure to flooding and tropical cyclones, understanding the interplay between multiple flood drivers is crucial.

Extreme coastal flooding events frequently involve compound hazards, where storm surge, riverine flooding, and heavy rainfall may interact to amplify impacts. Compound coastal flooding poses considerable challenges for prediction and hazard assessment, especially in low-relief coastal regions. Compound events are natural hazards that co-occur over time or space and threaten society and the environment (Zscheischler et al., 2020). Coastal residents are particularly vulnerable to compound coastal flooding, which arises from the interaction of storm surge, fluvial flooding, and pluvial flooding, which are often triggered by tropical cyclones (Green et al., 2025). Compound floods can lead to more severe impacts than floods caused by a single driver (Bevacqua et al., 2020; Hao and Singh, 2020). The primary drivers of compound coastal flooding–coastal water levels, precipitation, and river flow–are interdependent and inherently correlated (Zheng et al., 2013; Wahl et al., 2015; Moftakhari et al., 2017; Hendry et al., 2019). These mechanisms can act simultaneously or sequentially, leading to dynamic interactions that amplify flood hazards. Predicting compound coastal flooding is particularly challenging in low-relief flood transition zones, where hydrologic and coastal flood drivers interact in a nonlinear manner (Shen et al., 2019; Bilskie et al., 2021; Santiago-Collazo et al., 2024). Storm surge, driven by strong winds and low atmospheric pressure, raises coastal water levels, which can impede river discharge, leading to backwater effects and prolonged inland flooding (Santiago-Collazo et al., 2019). Similarly, heavy precipitation can saturate soils, reducing infiltration and exacerbating runoff, while high tides and waves can further elevate water levels (Bilskie and Hagen, 2018).

Accurate flood prediction is essential for flood management; however, no single modeling approach is ideally suited to capture compound coastal flood events. Researchers and policymakers use three broad categories of flood inundation models to support decision-making: empirical methods, hydrodynamic models, and simplified conceptual models (Teng et al., 2017). These models address flood-related challenges in planning, impact assessment, and emergency response (Bates, 2022). Each approach has strengths and limitations that influence its applicability.

Empirical methods produce direct observations of flooding, including remote sensing, sensor data, and crowdsourced information (Tellman et al., 2021; Hamidi et al., 2023; Silverman et al., 2022; Dasgupta et al., 2022). While invaluable for planning and post-event assessments, these methods are less applicable to real-time decision support and compound flood analysis.

Hydrodynamic models estimate flow using the Navier-Stokes equations, making them widely adopted for flood simulations (Bates, 2022). To balance accuracy and efficiency, hydrodynamic modelers often simplify the Navier-Stokes equations, using two-dimensional shallow-water or one-dimensional Saint-Venant formulations (Westerink et al., 1992; Horritt and Bates, 2002; USACE, 2025). Coupled hydrodynamic models have been developed to describe compound flood processes, with some tools optimized for computational efficiency (Leijnse et al., 2021). However, computational demands limit hydrodynamic models' applicability to real-time or high-resolution scenarios (Santiago-Collazo et al., 2019; Miura et al., 2021).

Simplified conceptual models use physical principles, geographic information systems (GIS), and terrain analysis to estimate flood extent and depth efficiently (Teng et al., 2017; Bates, 2022). These models do not explicitly simulate flood dynamics but can approximate compound flooding using available topographic and hydrologic data. Some simplified conceptual models

https://doi.org/10.5194/egusphere-2026-577
Preprint. Discussion started: 20 February 2026

distribute water volume across terrain (Lhomme et al., 2009; Miura et al., 2021; Shi et al., 2025), while others classify floodplains based on digital elevation models (Nardi et al., 2006; Manfreda et al., 2011; Samela et al., 2017). Simplified conceptual models enable large-scale, high-resolution flood hazard assessments and support rapid decision-making in emergency response scenarios (Preisser et al., 2023; Jafarzadegan et al., 2023).

In this study, we employ two approaches to predict compound flooding: a) superimpose individual simplified conceptual models of fluvial, pluvial, and coastal flooding (Preisser et al., 2022; Zheng et al., 2018; Wang et al., 2024); and b) use SFINCS, a hydrodynamic model that captures fluvial, pluvial, and coastal flooding (Leijnse et al., 2021; Lee et al., 2025). Simplified models can rapidly generate synthetic flood inundation scenarios and are attractive for planning assessments of flood hazard (Murphy et al., 2025). SFINCS provides a benchmark hydrodynamic simulation that we compare with the simplified model results. We use these models to develop a framework for quantifying compound flood depth at points of interest (POIs).

This study aims to quantify compound flood depth at POIs given ranges of possible coastal flood drivers. We model our approach on the rating curve, which depicts stage as a function of river discharge at a river gage location, and is used to communicate compound flood impacts with planners, flood managers, and stakeholders. Recognizing that compound flood depth, which is analogous to stage height in a rating curve, depends on contributions from three flood drivers in coastal areas: precipitation, coastal water level, and river discharge, we restructure the rating curve to consider any two of these three drivers and plot their corresponding two-dimensional contours of compound flood depth at any POI. Though we model up to three coastal flood drivers at each POI, we plot rating surfaces as two-dimensional contours of compound flood depth to present multiple data sources simply and clearly. Our approach is similar to the fluvial-coastal surfaces for water levels in navigation channels proposed by Muñoz et al. (2022). We generate high-resolution (1 m) compound flood inundation scenarios using public datasets and open-source flood models, extending this concept and providing a general framework for assessing compound flood depth at POIs.

2 Methods

2.1 Study areas

Our study areas are the inland town of Silsbee and the coastal city of Port Arthur, both located in Southeast Texas on low-relief topography susceptible to coastal compound flooding (Fig. 1). We choose POIs within regions designated as flood-prone by local stakeholders working with the Southeast Texas Urban Integrated Field Laboratory (SETx-UIFL, 2024). POIs in the study areas are situated near socially vulnerable populations and critical energy infrastructure. The Southeast Texas region encompasses the Beaumont-Port Arthur metropolitan area, smaller towns like Silsbee, agricultural lands, forests, and swamps. Tropical cyclones including Beryl (2024), Imelda (2019), and Harvey (2017) have impacted the area. The region is drained by the Sabine, Neches, and Trinity Rivers and their tributaries. Terrain slopes gently toward the Gulf of Mexico, which is typical of the Texas Coastal Plains. The area contains Galveston Bay and Sabine Lake.

https://doi.org/10.5194/egusphere-2026-577
Preprint. Discussion started: 20 February 2026

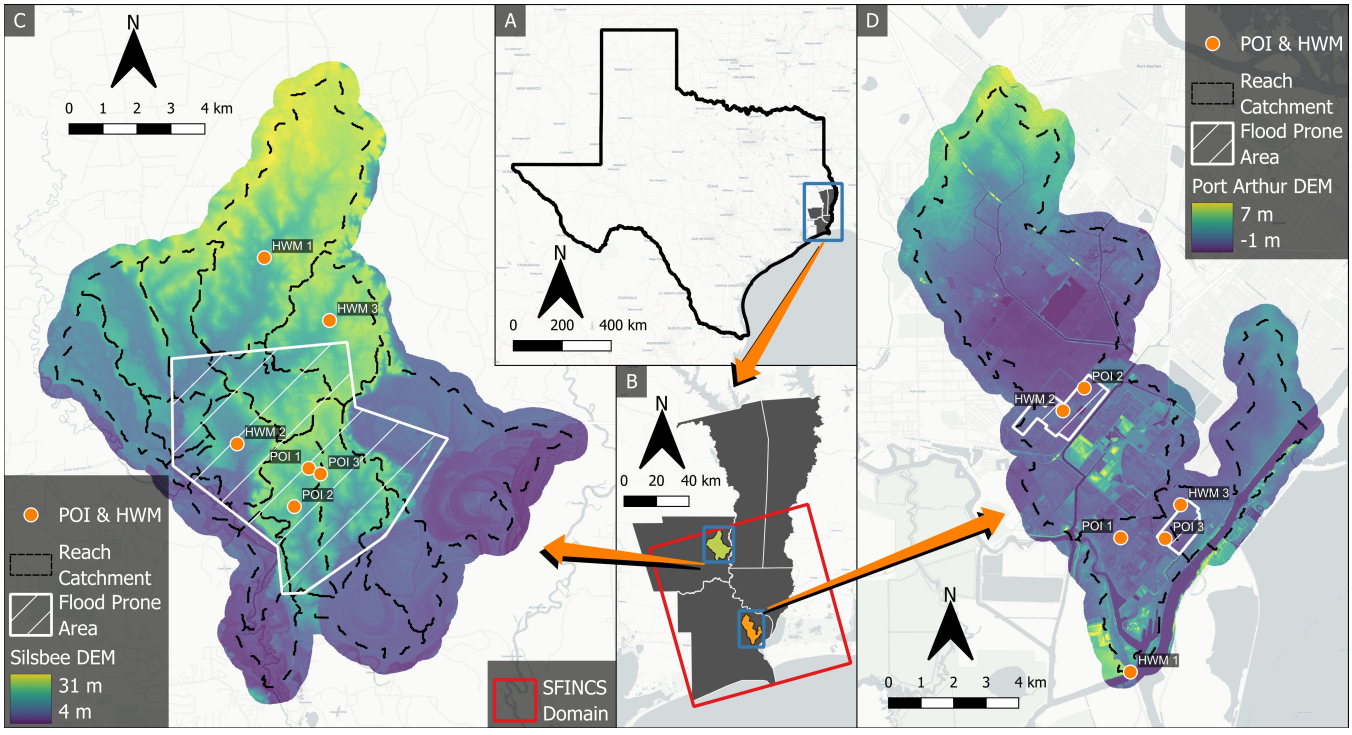

Figure 1. Location of (A) Southeast Texas within the state of Texas, (B) the Silsbee and Port Arthur study areas within Southeast Texas, as well as the SFINCS domain, (C) the Silsbee study area extent and datasets, and (D) the Port Arthur study area extent and datasets. Basemap © OpenStreetMap contributors, © CARTO.

2.2 Simplified conceptual models

c-HAND produces coastal flood inundation scenarios (Wang et al., 2024). c-HAND is a static method that uses high-resolution elevation data and a coastal water level forecast to estimate coastal flood extent and depth. It is a modification of the HAND method and estimates coastal inundation by enforcing an ocean connectivity constraint. A c-HAND backcast of coastal inundation from Hurricane Ike showed reasonable agreement with an ADCIRC simulation (Wang et al., 2024). We force c-HAND with coastal water levels (Sec. 2.5.1).

We generate synthetic fluvial flood inundation scenarios with a modification of the GeoFlood workflow (Zheng et al., 2018). GeoFlood has been used to model fluvial inundation extent and depth from Hurricane Harvey (Zheng et al., 2022). We force GeoFlood with synthetic river discharge scenarios (Sec. 2.5.2) in the NHDPlusV2 MR stream reach catchments containing our POI/HWM.

We estimate pluvial flooding with Fill-Spill-Merge, a terrain depression flow routing algorithm that can be applied to a broad range of natural phenomena (Barnes et al., 2021). Fill-Spill-Merge has been used to map pluvial flooding in Texas (Preisser et al., 2022, 2023). We force Fill-Spill-Merge with uniform precipitation depths (Sec. 2.5.3). Because Fill-Spill-Merge does not

https://doi.org/10.5194/egusphere-2026-577
Preprint. Discussion started: 20 February 2026

take drainage infrastructure or infiltration into account, we assume that soil is saturated and the drainage system is at capacity, which is likely for large precipitation events in Southeast Texas.

2.2.1 Compound flood depth with simplified conceptual models

We produce 1 m resolution coastal, fluvial, and pluvial flood depth grids separately across the study area with the models described above. The depth grid for each forcing corresponds to the maximum inundation depth and extent achieved under that forcing. To approximate compound flood depth at each POI/HWM, we superimpose the estimated depths from two forcing scenarios (Eq. 1–3):

$$h_{\text{fluvial}-\text{pluvial}} = h_{\text{pluvial}} + h_{\text{fluvial}} \tag{1}$$

$$h_{\text{coastal}-\text{pluvial}} = \max\left(h_{\text{coastal}}, h_{\text{pluvial}}\right) \tag{2}$$

$$h_{\text{fluvial}-\text{coastal}} = \max\left(h_{\text{coastal}}, h_{\text{fluvial}}\right) \tag{3}$$

where $h_{\text{fluvial}-\text{pluvial}}$ is the compound fluvial-pluvial flood depth, $h_{\text{coastal}-\text{pluvial}}$ is the compound coastal-pluvial flood depth, $h_{\text{fluvial}-\text{coastal}}$ is the compound fluvial-coastal flood depth, h_{fluvial} is the fluvial flood depth, h_{pluvial} is the pluvial flood depth, and h_{coastal} is the coastal flood depth.

We use the compound flood depths resulting from Eq. 1–3 to construct rating surfaces for pairs of forcings at each POI/HWM. We sum pluvial and fluvial inundation because fluvial inundation is calculated on a depression-removed DEM and pluvial inundation is calculated on a DEM including depressions. We take the maximum of coastal and both fluvial and pluvial inundation because coastal inundation acts as a downstream boundary condition that controls water surface elevations across low-lying terrain. This approach yields a conservative lower-bound estimate of compound flood depth, as the interaction between coastal and inland flooding is nonlinear (Bilskie and Hagen, 2018).

2.3 SFINCS model setup

The SFINCS model domain spans 1000 × 1000 km and uses a 50 × 50 m regular grid with a 1 × 1 m subgrid scheme that resolves fine-scale topography (van Ormondt et al., 2025). We mosaic the topography and bathymetry datasets to cover the full SFINCS domain (Fig. 2). We apply outflow boundary conditions at domain edges intersecting land and constant water level boundary conditions at domain edges intersecting the ocean. We assign inflow boundary conditions where stream reaches intersect the model boundary and at headwaters within the domain. The subgrid tables include NHDPlusV2 MR stream reach centerline geometry, bankfull width and depth, and channel roughness, as well as land cover-based roughness outside of stream reaches. We disable infiltration in SFINCS to reduce systematic model bias and maintain consistency with the simplified conceptual models, which omit infiltration. Infiltration is also unlikely to have a strong influence on maximum depths at our POIs, which are located on impervious surfaces. We run seven-day SFINCS simulations with coastal, pluvial, and fluvial forcing scenarios.

https://doi.org/10.5194/egusphere-2026-577
Preprint. Discussion started: 20 February 2026

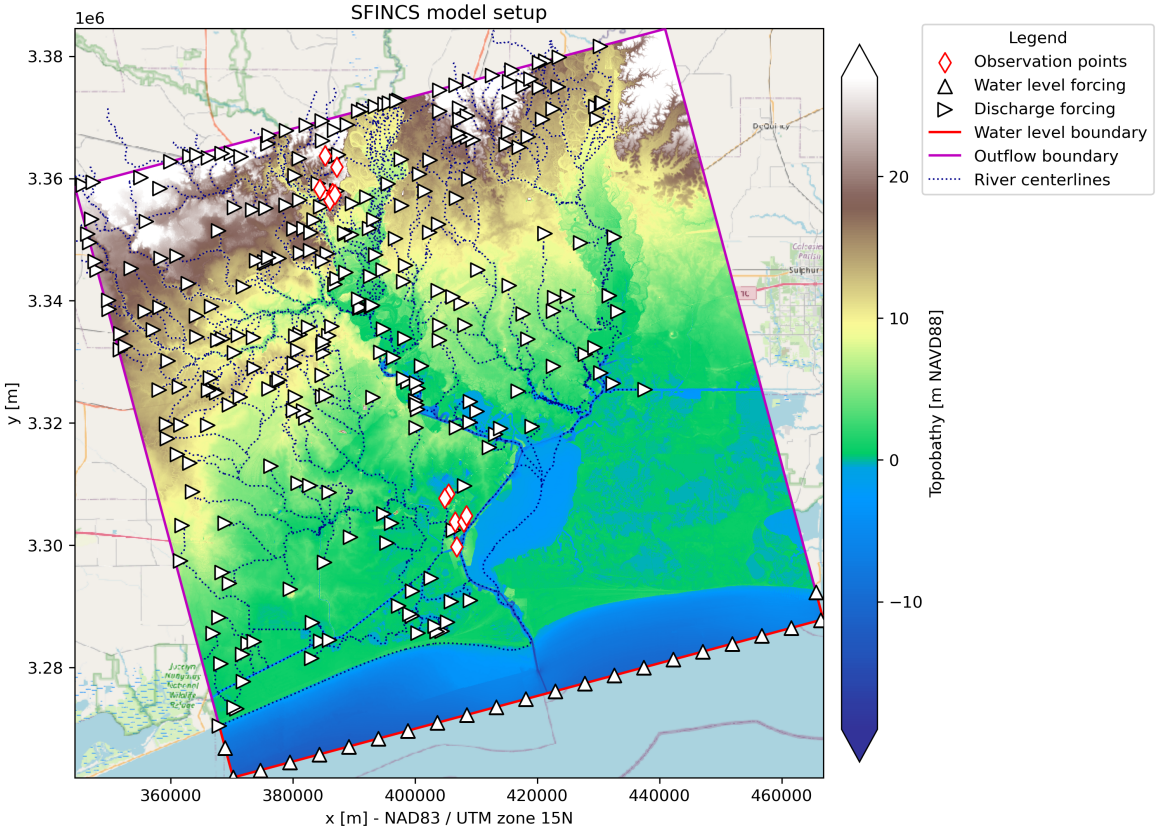

Figure 2. SFINCS model setup. Basemap © OpenStreetMap contributors.

2.3.1 SFINCS compound scenario selection

We generate compound flooding scenarios by pairing coastal, fluvial, and pluvial forcings across their full ranges (Sec. 2.5.1–2.5.3). SFINCS receives each forcing combination as a seven-day simulation that shares a common domain, boundary setup, and subgrid configuration. The only difference among SFINCS scenario setups is the choice of forcing magnitudes.

For each pair of flood drivers, we construct a continuous two-dimensional forcing space, discretized with a deterministic Halton sequence (Halton, 1960). The Halton sequence distributes sample points uniformly across the forcing space. We hold the third driver at a constant low value so that maps are representative of the inundation resulting from two drivers as with the simplified conceptual models (Table 1). We set coastal water level to 0 m NAVD88 for fluvial-pluvial scenarios, which falls between mean low water (-0.07 m NAVD88) and mean sea level (0.07 m NAVD88) at the Port Arthur tide gage. We set discharge to baseflow for coastal-pluvial scenarios and set precipitation depth to 0 mm for fluvial-coastal scenarios.

We generate 1000 forcing combinations for each pair of drivers. The three forcing grids (fluvial–pluvial, coastal–pluvial, and coastal–fluvial) span the full ranges of coastal water level, maximum discharge, and precipitation depth. The Halton-sampled

https://doi.org/10.5194/egusphere-2026-577
Preprint. Discussion started: 20 February 2026

Table 1. SFINCS compound scenario types and corresponding forcing ranges.

	Forcings		
Scenario type	Coastal [m NAVD88]	Fluvial[a] [$m^3 s^{-1}$]	Pluvial [mm]
Fluvial–pluvial	0	25 to 20000	10 to 300
Coastal–pluvial	0.1 to 2.0	baseflow	10 to 300
Fluvial–coastal	0.1 to 2.0	25 to 20000	0

[a] Represents maximum discharge within the watershed.

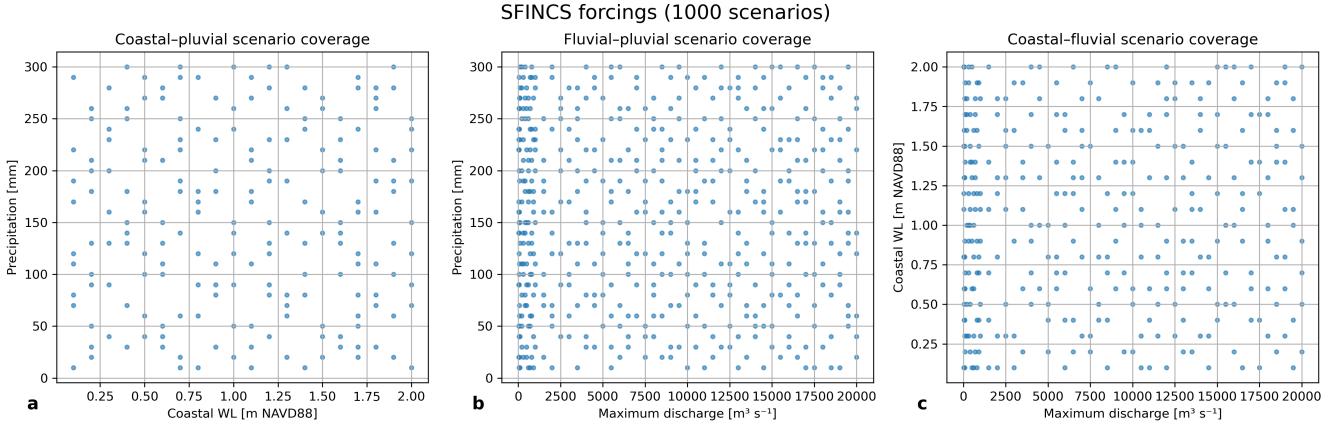

Figure 3. Halton-sequence coverage of compound forcing spaces used for SFINCS simulations. The three panels show 1000 forcing combinations across each pair: (A) coastal-pluvial, (B) fluvial-pluvial, and (C) fluvial-coastal. Apparent clustering near zero discharge reflects the non-uniform spacing of fluvial forcing magnitudes, where resolution at low flows is increased (Sec. 2.5.2)

points evenly fill each forcing space (Fig. 3). This approach provides broad coverage while keeping the total number of SFINCS simulations computationally feasible.

Each SFINCS run produces a time series of water surface elevation on the 50 m grid. We compute the maximum value over the full seven-day period at every coarse grid cell and downscale the coarse maximum water surface grid to a 1 m depth grid. We sample the 1 m maximum depth grid at each POI/HWM. The sampled depths form the inputs to the rating-surface construction (Sec. 2.6).

2.4 Datasets

We obtain 1 m resolution bare-earth digital elevation models (DEM) from the USGS 3D Elevation Program for Silsbee and areas outside of Jefferson County (USGS, 2024) and from the TNRIS StratMap Program for Port Arthur and areas within Jefferson County (TNRIS, 2017) (Fig. 1). We obtain bathymetry with the finest available resolution of 4 m from NOAA

https://doi.org/10.5194/egusphere-2026-577
Preprint. Discussion started: 20 February 2026

Table 2. High-water mark (HWM) and point-of-interest (POI) information.

Site	Location	Type
Port Arthur POI 1[a]	S Gulfway Dr & Valero Refinery Gates	Industrial
Port Arthur POI 2	Linkwood St & Austin Ave	Residential
Port Arthur POI 3	W 10th St & Herget Ave	Residential
Port Arthur HWM 1[a]	Under West Port Arthur Bridge	Bridge crossing
Port Arthur HWM 2	Back of St John's Catholic Church	Drainage swale
Port Arthur HWM 3	Across from Booker T. Washington Elementary	Drainage swale
Silsbee POI 1[a]	Hwy 96 & FM 327	Downtown
Silsbee POI 2	Maxwell Dr & Lindsey	Residential
Silsbee POI 3	Watts Rd & FM 327	Highway underpass
Silsbee HWM 1	Upstream side of bridge on FM 1122	Bridge crossing
Silsbee HWM 2	Upstream of culvert on FM 327	Culvert crossing
Silsbee HWM 3[a]	Downstream of bridge on FM 92	Bridge crossing

[a] Located on or adjacent to a TxDOT-designated evacuation route.

BlueTopo (NOAA, 2025a). We delineate the coastline using U.S. Census TIGER/Line data (US Census Bureau, 2025). All geospatial datasets reference UTM Zone 15N coordinates (EPSG:26915) and the NAVD88 vertical datum (EPSG:5103).

Stream reaches, gage adjusted mean annual flow for each stream reach, and stream reach catchments are from the National Hydrography Dataset Version 2 Medium Resolution (NHDPlusV2 MR) Dataset, which is maintained by the USGS (McKay et al., 2012). The National Water Model (NWM) provides historical flow rates (Cosgrove et al., 2024) and the USGS provides hydraulic geometry estimates including bankfull width and depth (Schwarz et al., 2018) for each NHDPlusV2 MR stream reach. We assign channel Manning's n by stream order following GeoFlood's current implementation, and where stream order is unavailable we assign n to 0.03. Outside of stream channels, we assign roughness based on the 2023 National Land Cover Database 30 m dataset (USGS, 2025) with recommended land cover class–Manning's n mappings from the HEC-RAS manual (USACE, 2025).

We calculate rating surfaces at 12 point locations: three POIs and three HWMs in both Silsbee and Port Arthur (Table 2). We select POIs at locations where estimating compound flood depth for specific combinations of hydrological forcings is important for identifying management strategies. POI are located in residential areas, along hurricane evacuation routes (TxDOT, 2025), and near critical infrastructure (Fig. 1). USGS collected the HWMs after Hurricane Harvey (USGS and Arctur, 2018).

For model validation, we use observed forcing magnitudes from Hurricane Harvey. Peak stream segment discharges were 6140 $\mathrm{m^3\,s^{-1}}$ at Silsbee and 14440 $\mathrm{m^3\,s^{-1}}$ at Port Arthur according to NWM retrospective data. Coastal water level at the Port Arthur tide gage reached 1.13 m NAVD88. The National Hurricane Center reported 173 mm of rainfall within one hour over Southeast Texas (Blake and Zelinsky, 2018). This depth corresponds to the 1000 yr, 1 h event at Beaumont (NOAA, 2025b),

https://doi.org/10.5194/egusphere-2026-577
Preprint. Discussion started: 20 February 2026

which we adopt as the representative precipitation depth for validation. These values are used as inputs to the rating surfaces to evaluate modeled flood depths against the observed high-water marks.

2.5 Compound flood forcings

2.5.1 Coastal

We apply coastal water levels ranging from 0 m to 2.0 m by increments of 0.1 m. The maximum water surface elevation measured by the NOAA tide gage at Port Arthur (Station 8770475) is 1.13 m (record begins in 2004). c-HAND calculates a static maximum coastal inundation map for each coastal water level, while we force SFINCS with a constant coastal water level throughout each seven-day simulation and obtain the corresponding downscaled maximum inundation maps.

2.5.2 Fluvial

We generate fluvial scenarios consisting of discharge ensembles. First we obtain gage-adjusted mean annual discharge from the NHDPlusV2 EROM dataset (US EPA, 2015). Then we assign discharge to each stream reach based on its mean annual discharge relative to the minimum and maximum in the study area, resulting in a vector of normalized discharges ranging from 0 to 1 (Eq. 4). We multiply this vector by a constant value to generate a corresponding synthetic discharge scenario (Eq. 5):

$$Q_{i,\mathrm{norm}} = \frac{Q_i - Q_{\min}}{Q_{\max} - Q_{\min}} \quad \forall\, i \tag{4}$$

$$\boldsymbol{Q}_{\mathrm{scenario}} = C \times \boldsymbol{Q}_{\mathrm{norm}} \tag{5}$$

where $Q_{i,\mathrm{norm}}$ is the normalized discharge at stream segment i, Q_i is mean annual discharge at stream segment i, $Q_{\min}$ is the minimum mean annual discharge of a stream segment in the study area, $Q_{\max}$ is the maximum mean annual discharge of a stream segment in the study area, $\boldsymbol{Q}_{\mathrm{scenario}}$ is the vector of discharges corresponding to a synthetic discharge ensemble, C is the scaling factor corresponding to the maximum discharge ($\mathrm{m^3\,s^{-1}}$) for a given synthetic scenario, and $\boldsymbol{Q}_{\mathrm{norm}}$ is a dimensionless vector of the normalized discharges at each stream segment. We force GeoFlood and SFINCS using fluvial scenarios defined by scaling factors C corresponding to maximum discharges ranging from 25 $\mathrm{m^3\,s^{-1}}$ to 20000 $\mathrm{m^3\,s^{-1}}$ (from less than baseflow to greater than Harvey)[1]. GeoFlood produces a static maximum inundation map associated with each fluvial scenario, while we force SFINCS with each constant fluvial scenario throughout each seven-day simulation and obtain the corresponding downscaled maximum inundation maps.

To validate the discharge scaling method, we compare scaled synthetic discharges with maximum NWM discharges from three major flood events in Southeast Texas–Hurricane Ike, Hurricane Harvey, and Tropical Storm Imelda–as well as baseflow

[1] C [$\mathrm{m^3\,s^{-1}}$]: 25, 50, 75, 100, 200, 300, 400, 500, 600, 700, 800, 900, 1000, 1500, 2000, 2500, 3000, 3500, 4000, 4500, 5000, 5500, 6000, 6500, 7000, 7500, 8000, 8500, 9000, 9500, 10000, 10500, 11000, 11500, 12000, 12500, 13000, 13500, 14000, 14500, 15000, 15500, 16000, 16500, 17000, 17500, 18000, 18500, 19000, 19500, 20000.

https://doi.org/10.5194/egusphere-2026-577
Preprint. Discussion started: 20 February 2026

conditions. We evaluate the comparison using normalized root mean square error (nRMSE) between scaled synthetic and observed NWM peak discharges across stream reaches:

$$\mathrm{RMSE} = \sqrt{\frac{1}{n}\sum_{i=1}^{n}(Q_{\mathrm{pred},i} - Q_{\mathrm{obs},i})^2} \tag{6}$$

$$\mathrm{nRMSE} = \frac{\mathrm{RMSE}}{\overline{Q}_{\mathrm{obs}}} \tag{7}$$

where $Q_{\mathrm{pred},i}$ and $Q_{\mathrm{obs},i}$ are the predicted (synthetic) and observed (NWM) peak discharges at stream segment i, respectively, n is the number of stream segments, and $\overline{Q}_{\mathrm{obs}}$ is the mean of the observed peak discharges across a site. We report nRMSE as a dimensionless measure of model performance to clearly compare events across different magnitudes and sites. The nRMSE values range from 0.03 to 0.33 (Fig. S1), indicating that the discharge scaling method provides an efficient, approximate technique for systematic generation of multiple synthetic fluvial scenarios.

2.5.3 Pluvial

We generate pluvial scenarios with total precipitation depths ranging from 10 mm to 300 mm, incremented by 10 mm. Fill-Spill-Merge calculates a static maximum inundation map for each depth, while we force SFINCS with precipitation time series corresponding to each depth. SFINCS requires a precipitation time series rather than a total depth, which we derive using the NOAA precipitation depth-duration-frequency (DDF) table for Beaumont (Station ID 41-0611), at the geographic midpoint between Silsbee and Port Arthur (NOAA, 2025b).

To generate the precipitation time series for each scenario, we assign an annual recurrence interval (ARI) ranging from 1 yr to 1000 yr, with larger ARI values assigned to larger depths (Fig. S2). We then enter the DDF table with the scenario's ARI (frequency) and depth, using regular grid interpolation to extract the corresponding duration. The time series consists of the constant precipitation intensity that applies the scenario's depth over its interpolated duration, and the calculated intensity is applied at the beginning of the simulation.

For example, we assign a 2 yr ARI to the 50 mm scenario. Interpolating the DDF table, we determine this ARI and depth combination correspond to a storm duration of 0.7 h at Beaumont. The constant intensity needed to apply 50 mm of precipitation over 0.7 h is 71.43 $\mathrm{mm\,h^{-1}}$. The precipitation time series we supply to SFINCS for the 50 mm scenario consists of 71.43 $\mathrm{mm\,h^{-1}}$ for the first 0.7 h of the seven-day simulation, followed by 0 $\mathrm{mm\,h^{-1}}$ for the remainder of the simulation. We repeat this process for each pluvial scenario.

2.6 Rating surfaces

We define rating surfaces as contour plots of compound flood depth generated from pairwise combinations of flood drivers. We first estimate compound flood inundation across a range of forcing combinations and magnitudes, and then construct rating surfaces by sampling the resulting high-resolution maximum depth grids at POI/HWM. Two-dimensional contours

https://doi.org/10.5194/egusphere-2026-577
Preprint. Discussion started: 20 February 2026

of depth illustrate the response to variation in two flood drivers at a fixed location while the third driver remains constant. We apply Gaussian smoothing with $\sigma = 3$ to reduce small-scale noise in the interpolated SFINCS rating surfaces (Virtanen et al., 2020). Simplified conceptual model rating surfaces remain unsmoothed because they exhibit linear patterns without noise. Representing compound flood depth as a function of three forcings is possible, but pairwise contours, which represent compound flood depth as a function of two forcings, improve interpretability and clarify individual and joint effects.

3 Results

We evaluate compound flood rating surfaces generated from simplified conceptual models (SCM) and SFINCS to compare how each modeling approach represents flood depth responses to varying forcings. For each of the three forcing pairs, the rating surfaces summarize maximum flood depth at POI/HWM across identical ranges of precipitation, river discharge, and coastal water level (Figs. 4–6). SCM and SFINCS rating surfaces show similar broad patterns across most locations. SCM capture smooth, linear depth gradients, while SFINCS introduces finer variability and nonlinear patterns. We also validate the rating surfaces approach by comparing flood depths extracted from rating surfaces with observed HWM depths.

Compound flood depth rating surfaces from coastal–pluvial forcing combinations (Fig. 4) show that maximum flood depth at Port Arthur increases primarily with coastal water level and more modestly with precipitation. At inland Silsbee, maximum flood depth is largely insensitive to coastal water level and varies mainly with precipitation. The overall depth ranges are similar between SCM and SFINCS at each POI/HWM.

Rating surfaces for fluvial-coastal forcing combinations (Fig. 5) again indicate that coastal water level controls maximum flood depth at Port Arthur, with river discharge exerting only minor influence. At Silsbee the pattern reverses with river discharge accounting for most of the variation in maximum flood depth. Depth ranges are comparable between SCM and SFINCS at most POI/HWM, though SCM produces greater depths than SFINCS at Silsbee POI 1 and 2.

For fluvial–pluvial forcing combinations (Fig. 6), SFINCS-derived rating surfaces show maximum flood depth increasing primarily with precipitation. In contrast, SCM-derived surfaces show maximum flood depth varying with both precipitation and river discharge. The ranges of maximum flood depth are similar between SCM and SFINCS at roughly half of the POI/HWM, with the largest differences again occurring at Silsbee POI 1 and 2.

We validate the rating surfaces approach by comparing predicted flood depths against observed Hurricane Harvey HWMs in Port Arthur and Silsbee (Fig. 7). At each site we extract predicted depths from SCM and SFINCS derived rating surfaces using forcing magnitudes observed during Hurricane Harvey (maximum coastal water level, river discharge, and 1-hour precipitation depth). At Port Arthur, depth errors range from -0.52 m to 0.56 m with SCM and -0.52 m to 0.56 m with SFINCS. At Silsbee, depth errors range from -0.53 m to 2.26 m with SCM and -0.53 m to 1.99 m with SFINCS. With the exceptions of HWM 2 at Port Arthur and HWM 3 at Silsbee, observed HWMs lie within the envelope of depths predicted across the three forcing combinations.

https://doi.org/10.5194/egusphere-2026-577
Preprint. Discussion started: 20 February 2026

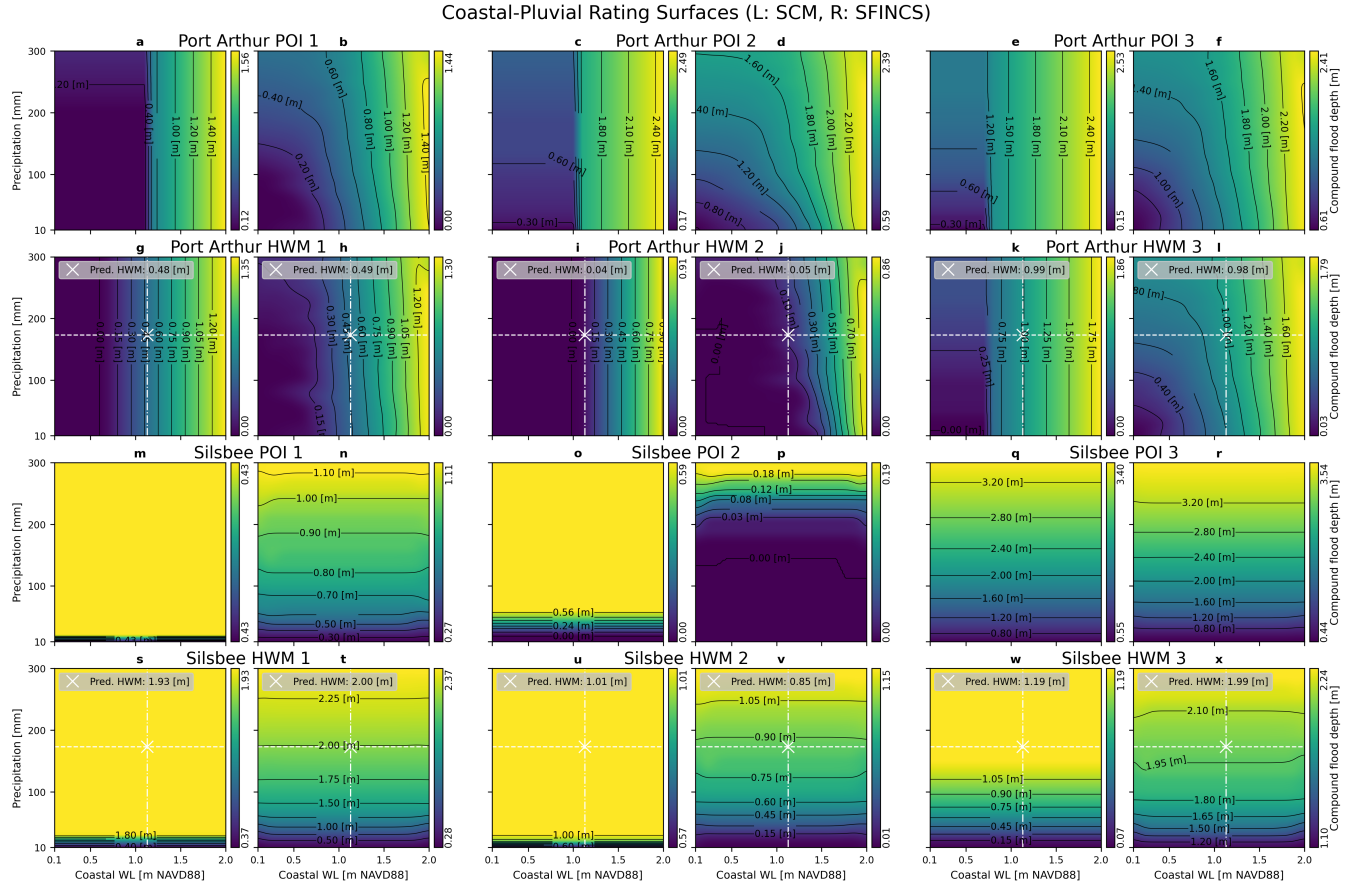

Figure 4. Coastal–pluvial rating surfaces derived from simplified conceptual models (SCMs; left columns) and SFINCS (right columns). Panels show compound flood depth as a function of coastal water level and precipitation across POI/HWM in both study areas.

4 Discussion

Coastal-pluvial rating surfaces demonstrate the greatest agreement between SCM and SFINCS among the three forcing pairs. Each model shows the same broad patterns and depth ranges given varying coastal and pluvial forcings, with SFINCS exhibiting more refined variation due to its nonlinear representation of compounding effects (Fig. 4). Coastal-pluvial rating surfaces at Port Arthur (Fig. 4a-l) show that compound flood depth varies as a function of both precipitation rate and coastal water level, with the exceptions of SCM estimations at HWM 1 and 2, which vary only with coastal water level (Fig. 4g,i). This result is expected given Port Arthur's low-relief topography and proximity to the coast. At Silsbee, coastal-pluvial rating surfaces show compound flood depth varying with precipitation depth (Fig. 4m-x). While coastal inundation never reaches Silsbee, SFINCS (Fig. 4n,p,r,t,v,x) captures nonlinear effects that are missed by SCM (Fig. 4m,o,q,s,u,w), explaining the noisier contours in its rating surfaces.

https://doi.org/10.5194/egusphere-2026-577
Preprint. Discussion started: 20 February 2026

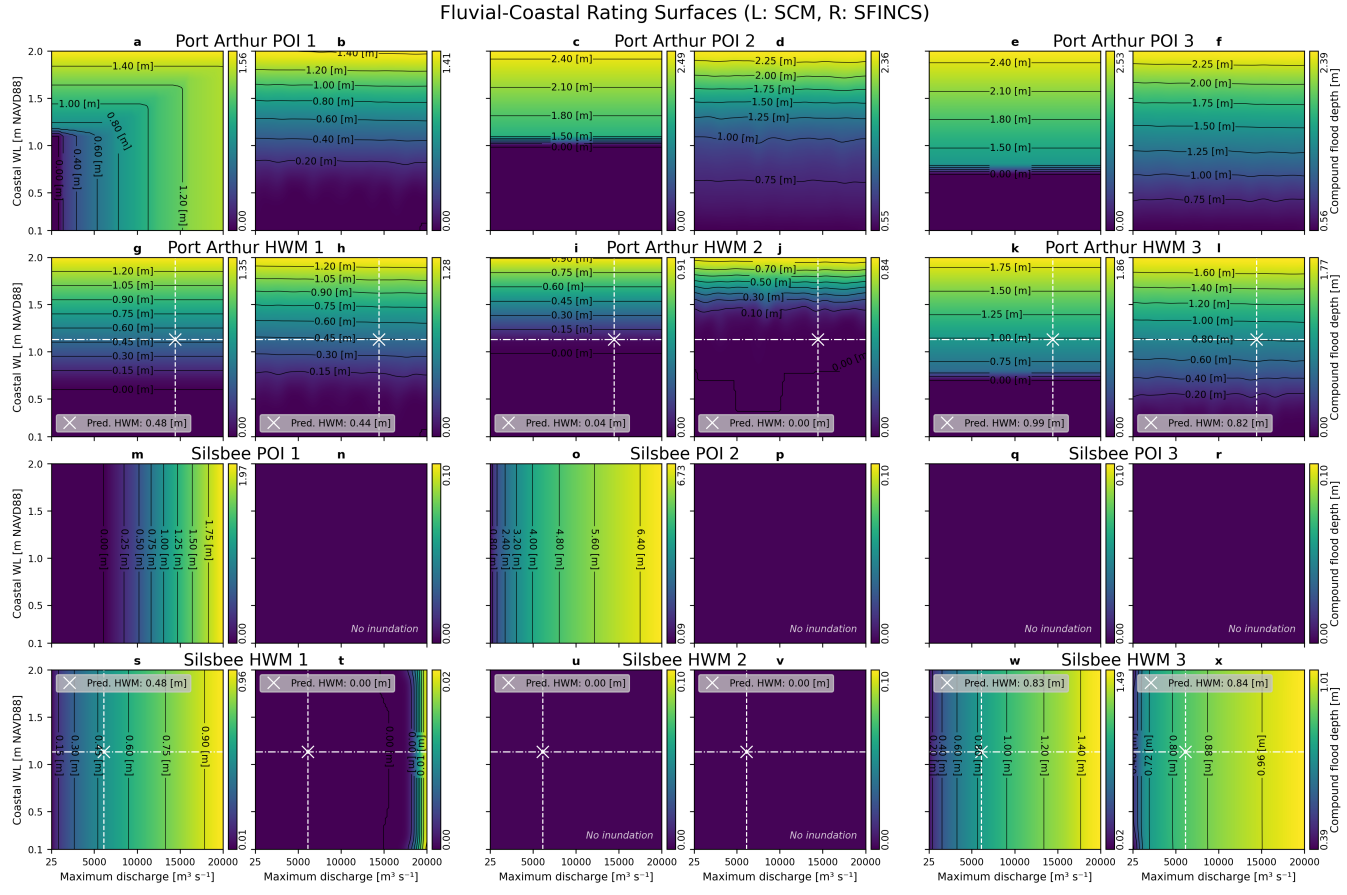

Figure 5. Fluvial–coastal rating surfaces derived from simplified conceptual models (SCMs; left columns) and SFINCS (right columns). Panels show compound flood depth as a function of maximum discharge and coastal water level across POI/HWM in both study areas.

Fluvial-coastal rating surfaces also show SCM and SFINCS capturing similar patterns of compound flood inundation (Fig. 5). Port Arthur fluvial-coastal rating surfaces (Fig. 5a-l) show compound flood depth dominated by coastal water level variation, with only SCM showing a river discharge effect at POI 1 (Fig. 5a). Conversely, Silsbee fluvial-coastal rating surfaces (Fig. 5m-x) show compound flood depth dominated by river discharge, which aligns with Silsbee's inland position relative to Port Arthur. Fluvial-coastal forcing pairs do not yield any inundation at several locations in Silsbee (Fig. 5n,p,q,r,u,v), suggesting that pluvial flooding is a more dominant regime at those locations. Silsbee POI 1 and 2 exhibit considerable deviations in rating surface depth range between SCM and SFINCS (Fig. 5m,o), with differences of nearly 2 m and 7 m, respectively. This difference is due to a known limitation of GeoFlood and the Height Above Nearest Drainage (HAND) method that causes increased inundation depth in isolated river segment catchments (Aristizabal et al., 2023).

Fluvial-pluvial rating surfaces show mixed agreement between SCM and SFINCS (Fig. 6). At Port Arthur, fluvial-pluvial rating surface depths (Fig. 6a-l) are mainly influenced by precipitation, with GeoFlood also showing river discharge contribut-

https://doi.org/10.5194/egusphere-2026-577
Preprint. Discussion started: 20 February 2026

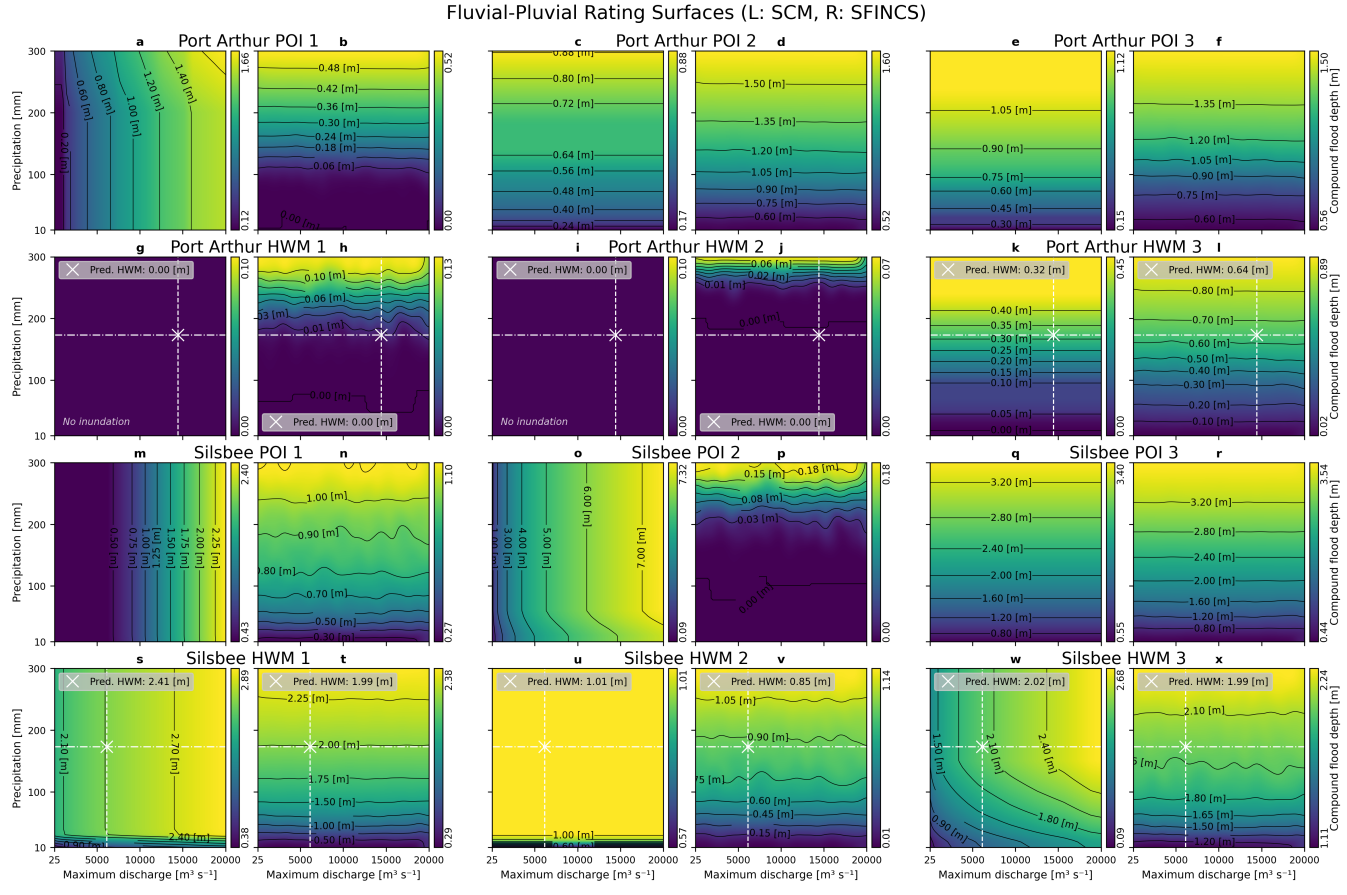

Figure 6. Fluvial–pluvial rating surfaces derived from simplified conceptual models (SCMs; left columns) and SFINCS (right columns). Panels show compound flood depth as a function of maximum discharge and precipitation across POI/HWM in the Port Arthur and Silsbee study areas.

ing to depth variation at POI 1 (Fig. 6a), where the terrain depression reaches capacity at a precipitation depth of around 200 mm. SCM and SFINCS produce zero or nearly-zero fluvial-pluvial compound inundation at Port Arthur POI 1 and 2. At Silsbee, SCM fluvial-pluvial rating surfaces show flood depth varying considerably with both fluvial and pluvial forcings, while SFINCS shows variation mainly with precipitation depth (Fig. 6m-x). POI 1 and 2 show greater deviations in rating surface depth range between SCM and SFINCS than we observed from the fluvial-coastal rating surfaces, with differences of $>$ 2 m and $>$ 7 m, respectively (Fig. 6m,o). We also attribute this discrepancy to the segment catchment limitation of HAND-GeoFlood. The deviations are greater here than for fluvial-coastal rating surfaces because we sum fluvial-pluvial SCM depth (GeoFlood is run on a depression-removed DEM, Fill-Spill-Merge is not) rather than taking the maximum. Interestingly, despite SCM and SFINCS predicting different fluvial-pluvial contributions to compound flood depth, the Silsbee HWM rating surfaces yield similar extracted depths using Hurricane Harvey forcings (Fig. 6s-x).

https://doi.org/10.5194/egusphere-2026-577
Preprint. Discussion started: 20 February 2026

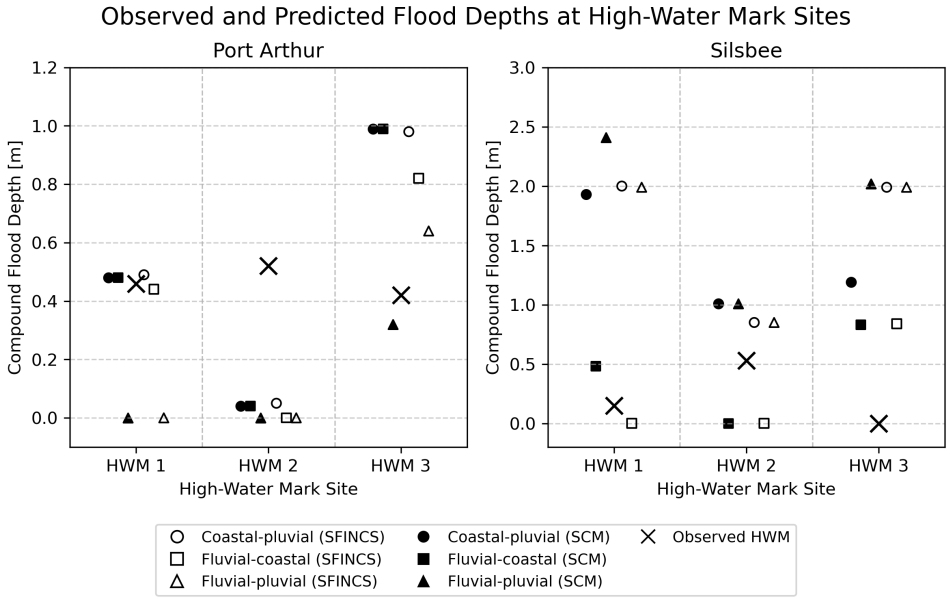

Figure 7. Observed and predicted high-water mark (HWM) flood depths at Port Arthur and Silsbee. Observed Harvey HWM depths are shown with predicted depths extracted from coastal–pluvial, fluvial–coastal, and fluvial–pluvial rating surfaces derived from SFINCS and simplified conceptual models (SCM).

To assess the accuracy of the rating surfaces approach, we select three HWMs collected during Hurricane Harvey for each study area and calculate rating surfaces at their locations (Figs. 4–6s–x). We extract predicted HWM elevations from each rating surface using the observed maximum fluvial, pluvial, and coastal forcings during Harvey (Sec. 2.4). Across both study areas, SCM and SFINCS predictions given the Harvey forcing combination are similar, even at sites where predicted and observed depths diverge, indicating that simplified models capture dominant patterns of hydrodynamic simulations despite their reduced physics. The largest discrepancies occur at the inland Silsbee sites, where pluvial and fluvial contributions are more uncertain due to low-relief topography and HWM collection near bridges and culverts. Additional uncertainty arises from the Harvey forcings themselves: peak rainfall rates exceeded many gage capacities (Blake and Zelinsky, 2018), NWM peak discharges carry uncertainty (Timilsina and Passalacqua, 2025), and small differences in local topography can shift HWM elevations.

The rating surface framework is model-agnostic, only requiring flood depth grids corresponding to compound flood driver forcings, which allows for flexibility in the choice of modeling techniques. Hydrodynamic models such as HEC-RAS and SFINCS capture physical processes with high fidelity when appropriately configured, but producing a large number of high-resolution scenarios is expensive, limiting accessibility and scale. Simplified conceptual models offer an efficient alternative, but lack the capability to simulate nonlinear and compound interactions among coastal, fluvial, and pluvial drivers. In this study SFINCS modeling cost nearly 6,000 node-hours on a supercomputer, while simplified models cost less than 100 node-hours.

https://doi.org/10.5194/egusphere-2026-577
Preprint. Discussion started: 20 February 2026

The accuracy of rating surfaces depends on the quality of underlying datasets and models. Missing or inaccurate hydrography can affect fluvial inundation representation. For example, the absence of an NHDPlusV2 MR flowline along part of the Sabine–Neches Waterway likely biased local fluvial depth estimates. Uncertainty in historical forcings also affects the accuracy of flood depths extracted from rating surfaces. In addition, low-relief terrain may cause HAND-GeoFlood to overestimate inundation (Johnson et al., 2019; Garousi-Nejad et al., 2019; Scriven et al., 2021; Richardson and Beighley, 2024). A natural extension of rating surfaces would be a pairing with joint probability models of compound drivers, as implemented in Dutch regulatory frameworks that summarize probabilistic flood hazards using two-dimensional sea level–discharge isolines corresponding to flood-defense failure thresholds (Geerse et al., 2011; Duits, M. T., 2004).

5 Conclusions

This study introduces rating surfaces as a method to quantify and visualize compound flood depth as a function of two interacting flood drivers at points of interest. We generate large ensembles of high-resolution inundation scenarios using both simplified conceptual models and a hydrodynamic model and sample these scenarios at POIs to construct rating surfaces. The resulting surfaces provide an interpretable representation of how local flood depth responds to combinations of precipitation, discharge, and coastal water level.

Rating surfaces from both modeling approaches capture relatively consistent first-order patterns across the range of forcings. Validation against Hurricane Harvey high-water marks shows that rating surfaces reproduce event-scale magnitudes within the limits of underlying topography, hydrography, and historical forcing uncertainties. The spatial variability we observe across nearby POIs underscores the importance of neighborhood-scale analyses and high-resolution elevation data when assessing flood hazards in developed low-lying areas. Future work could apply this framework to other geographic settings and storm events, incorporate additional hydrodynamic models, and evaluate the influence of improved hydrography and precipitation datasets. Rating surfaces are a flexible tool for representing compound flooding at locations of interest across diverse modeling environments.

Supplement. The supplement related to this article is available online at [x].

Code and data availability. All datasets used in this study are publicly available online from the USGS, TNRIS, NOAA, and the U. S. Census Bureau. pyGeoFlood (which implements GeoFlood, c-HAND, and Fill-Spill-Merge) and SFINCS are free and open-source software (https://passah2o.github.io/pygeoflood/, https://sfincs.readthedocs.io/en/latest/).

https://doi.org/10.5194/egusphere-2026-577
Preprint. Discussion started: 20 February 2026

Author contributions. MW obtained the datasets, performed the analysis, and wrote the original draft. PP and HM contributed to this study's conceptualization and design. PP, HM, and MW edited the draft. PP provided research supervision and funding acquisition. BH assisted with data analysis.

Competing interests. The contact author has declared that none of the authors has any competing interests.

Acknowledgements. We thank Dr. Wonhyun Lee of the Bureau of Economic Geology at UT Austin for his feedback on the SFINCS model, and the Texas Advanced Computing Center (TACC) at UT Austin for providing computational resources that have contributed to the research results reported within this paper. URL: http://www.tacc.utexas.edu

Financial support. This material is based upon work supported by the U.S. Department of Energy, Office of Science, Biological and Environmental Research Program under Award Number DE-SC0023216, the NOAA Adaptation Sciences Program (NOAA-OAR-CPO-2021-2006389), the Cockrell School of Engineering, and Planet Texas 2050, a research grand challenge at the University of Texas at Austin.

https://doi.org/10.5194/egusphere-2026-577
Preprint. Discussion started: 20 February 2026

References

Aristizabal, F., Salas, F., Petrochenkov, G., Grout, T., Avant, B., Bates, B., Spies, R., Chadwick, N., Wills, Z., and Judge, J.: Extending Height Above Nearest Drainage to Model Multiple Fluvial Sources in Flood Inundation Mapping Applications for the U.S. National Water Model, Water Resources Research, 59, e2022WR032 039, https://doi.org/10.1029/2022WR032039, 2023.

Barnes, R., Callaghan, K. L., and Wickert, A. D.: Computing water flow through complex landscapes - Part 3: Fill-Spill-Merge: Flow routing in depression hierarchies, Earth Surface Dynamics, 9, 105–121, https://doi.org/10.5194/esurf-9-105-2021, 2021.

Bates, P. D.: Flood Inundation Prediction, Annual Review of Fluid Mechanics, 54, 287–315, https://doi.org/10.1146/annurev-fluid-030121-113138, 2022.

Bevacqua, E., Vousdoukas, M. I., Zappa, G., Hodges, K., Shepherd, T. G., Maraun, D., Mentaschi, L., and Feyen, L.: More meteorological events that drive compound coastal flooding are projected under climate change, Communications Earth & Environment, 1, 1–11, https://doi.org/10.1038/s43247-020-00044-z, 2020.

Bilskie, M. V. and Hagen, S. C.: Defining Flood Zone Transitions in Low-Gradient Coastal Regions, Geophysical Research Letters, 45, 2761–2770, https://doi.org/10.1002/2018GL077524, 2018.

Bilskie, M. V., Zhao, H., Resio, D., Atkinson, J., Cobell, Z., and Hagen, S. C.: Enhancing Flood Hazard Assessments in Coastal Louisiana Through Coupled Hydrologic and Surge Processes, Frontiers in Water, 3, https://doi.org/10.3389/frwa.2021.609231, 2021.

Blake, E. S. and Zelinsky, D. A.: National Hurricane Center Tropical Cyclone Report: Hurricane Harvey, https://www.nhc.noaa.gov/data/tcr/AL092017_Harvey.pdf, 2018.

Cosgrove, B., Gochis, D., Flowers, T., Dugger, A., Ogden, F., Graziano, T., Clark, E., Cabell, R., Casiday, N., Cui, Z., Eicher, K., Fall, G., Feng, X., Fitzgerald, K., Frazier, N., George, C., Gibbs, R., Hernandez, L., Johnson, D., Jones, R., Karsten, L., Kefelegn, H., Kitzmiller, D., Lee, H., Liu, Y., Mashriqui, H., Mattern, D., McCluskey, A., McCreight, J. L., McDaniel, R., Midekisa, A., Newman, A., Pan, L., Pham, C., RafieeiNasab, A., Rasmussen, R., Read, L., Rezaeianzadeh, M., Salas, F., Sang, D., Sampson, K., Schneider, T., Shi, Q., Sood, G., Wood, A., Wu, W., Yates, D., Yu, W., and Zhang, Y.: NOAA's National Water Model: Advancing operational hydrology through continental-scale modeling, JAWRA Journal of the American Water Resources Association, 60, 247–272, https://doi.org/10.1111/1752-1688.13184, 2024.

Crossett, K., Ache, B., Pacheco, P., and Haber, K.: National Coastal Population Report, https://cdn.oceanservice.noaa.gov/oceanserviceprod/facts/coastal-population-report.pdf, 2013.

Dasgupta, A., Grimaldi, S., Ramsankaran, R., Pauwels, V. R. N., and Walker, J. P.: A simple framework for calibrating hydraulic flood inundation models using Crowd-sourced water levels, Journal of Hydrology, 614, 128 467, https://doi.org/10.1016/j.jhydrol.2022.128467, 2022.

Duits, M. T.: Handleiding Hydra-B – Geavanceerde gebruikers (versie 3.0), Rijkswaterstaat, 221559, https://open.rijkswaterstaat.nl/@167823/handleiding-hydra-geavanceerde/, 2004.

Dullaart, J. C. M., Muis, S., Bloemendaal, N., Chertova, M. V., Couasnon, A., and Aerts, J. C. J. H.: Accounting for tropical cyclones more than doubles the global population exposed to low-probability coastal flooding, Communications Earth & Environment, 2, 1–11, https://doi.org/10.1038/s43247-021-00204-9, 2021.

Garousi-Nejad, I., Tarboton, D. G., Aboutalebi, M., and Torres-Rua, A. F.: Terrain Analysis Enhancements to the Height Above Nearest Drainage Flood Inundation Mapping Method, Water Resources Research, 55, 7983–8009, https://doi.org/10.1029/2019WR024837, _eprint: https://onlinelibrary.wiley.com/doi/pdf/10.1029/2019WR024837, 2019.

https://doi.org/10.5194/egusphere-2026-577
Preprint. Discussion started: 20 February 2026

Geerse, C., Slomp, R, and de Waal, H: Hydra-Zoet for the fresh water systems in the Netherlands, Rijkswaterstaat, 501244, https://open.rijkswaterstaat.nl/@171393/hydra-zoet-probabilistic-model-for-the/, 2011.

Green, J., Haigh, I. D., Quinn, N., Neal, J., Wahl, T., Wood, M., Eilander, D., de Ruiter, M., Ward, P., and Camus, P.: Review article: A comprehensive review of compound flooding literature with a focus on coastal and estuarine regions, Natural Hazards and Earth System Sciences, 25, 747–816, https://doi.org/10.5194/nhess-25-747-2025, 2025.

Halton, J. H.: On the efficiency of certain quasi-random sequences of points in evaluating multi-dimensional integrals, Numerische Mathematik, 2, 84–90, https://doi.org/10.1007/BF01386213, 1960.

Hamidi, E., Peter, B. G., Muñoz, D. F., Moftakhari, H., and Moradkhani, H.: Fast Flood Extent Monitoring With SAR Change Detection Using Google Earth Engine, IEEE Transactions on Geoscience and Remote Sensing, 61, 1–19, https://doi.org/10.1109/TGRS.2023.3240097, conference Name: IEEE Transactions on Geoscience and Remote Sensing, 2023.

Hao, Z. and Singh, V. P.: Compound Events under Global Warming: A Dependence Perspective, Journal of Hydrologic Engineering, 25, 03120 001, https://doi.org/10.1061/(ASCE)HE.1943-5584.0001991, 2020.

Hendry, A., Haigh, I. D., Nicholls, R. J., Winter, H., Neal, R., Wahl, T., Joly-Laugel, A., and Darby, S. E.: Assessing the characteristics and drivers of compound flooding events around the UK coast, Hydrology and Earth System Sciences, 23, 3117–3139, https://doi.org/10.5194/hess-23-3117-2019, 2019.

Horritt, M. and Bates, P.: Evaluation of 1D and 2D numerical models for predicting river flood inundation, Journal of hydrology, 268, 87–99, 2002.

Jafarzadegan, K., Moradkhani, H., Pappenberger, F., Moftakhari, H., Bates, P., Abbaszadeh, P., Marsooli, R., Ferreira, C., Cloke, H. L., Ogden, F., and Duan, Q.: Recent Advances and New Frontiers in Riverine and Coastal Flood Modeling, Reviews of Geophysics, 61, e2022RG000 788, https://doi.org/10.1029/2022RG000788, 2023.

Johnson, J. M., Munasinghe, D., Eyelade, D., and Cohen, S.: An integrated evaluation of the National Water Model (NWM)–Height Above Nearest Drainage (HAND) flood mapping methodology, Natural Hazards and Earth System Sciences, 19, 2405–2420, https://doi.org/10.5194/nhess-19-2405-2019, 2019.

Lee, W., Sun, A. Y., and Scanlon, B. R.: Probabilistic storm surge and flood-inundation modeling of the Texas gulf coast using super-fast INundation of CoastS (SFINCS), Coastal Engineering, 198, 104 721, https://doi.org/10.1016/j.coastaleng.2025.104721, 2025.

Leijnse, T., van Ormondt, M., Nederhoff, K., and van Dongeren, A.: Modeling compound flooding in coastal systems using a computationally efficient reduced-physics solver: Including fluvial, pluvial, tidal, wind- and wave-driven processes, Coastal Engineering, 163, 103 796, https://doi.org/10.1016/j.coastaleng.2020.103796, 2021.

Lhomme, J., Sayers, P., Gouldby, B., Samuels, P., Wills, M., and Mulet-Marti, J.: Recent development and application of a rapid flood spreading method, in: Flood Risk Management: Research and Practice, pp. 15–24, Taylor & Francis Group, London, ISBN 978-0-415-48507-4, http://www.sayersandpartners.co.uk/uploads/6/2/0/9/6209349/2008_lhomme_sayers_et_al_-_recent_development_and_application_of_a_rapid_flood_spreading_method_floodrisk08.pdf, 2009.

Manfreda, S., Di Leo, M., and Sole, A.: Detection of Flood-Prone Areas Using Digital Elevation Models, Journal of Hydrologic Engineering, 16, 781–790, https://doi.org/10.1061/(ASCE)HE.1943-5584.0000367, 2011.

McKay, L., Bondelid, T., Dewald, T., Johnston, J., Moore, R., and Rea, A.: NHDPlus Version 2: User Guide, https://www.epa.gov/system/files/documents/2023-04/NHDPlusV2_User_Guide.pdf, 2012.

Miura, Y., Mandli, K. T., and Deodatis, G.: High-Speed GIS-Based Simulation of Storm Surge–Induced Flooding Accounting for Sea Level Rise, Natural Hazards Review, 22, 04021 018, https://doi.org/10.1061/(ASCE)NH.1527-6996.0000465, 2021.

https://doi.org/10.5194/egusphere-2026-577
Preprint. Discussion started: 20 February 2026

Moftakhari, H. R., Salvadori, G., AghaKouchak, A., Sanders, B. F., and Matthew, R. A.: Compounding effects of sea level rise and fluvial flooding, Proceedings of the National Academy of Sciences, 114, 9785–9790, https://doi.org/10.1073/pnas.1620325114, 2017.

Murphy, S., Wang, M., Cheng, C.-S., Passalacqua, P., and Leite, F.: Land-use analysis using infrastructure representations and high-resolution flood inundation mapping techniques, International Journal of Disaster Risk Reduction, 123, 105 518, https://doi.org/10.1016/j.ijdrr.2025.105518, 2025.

Muñoz, D. F., Moftakhari, H., Kumar, M., and Moradkhani, H.: Compound Effects of Flood Drivers, Sea Level Rise, and Dredging Protocols on Vessel Navigability and Wetland Inundation Dynamics, Frontiers in Marine Science, 9, https://doi.org/10.3389/fmars.2022.906376, 2022.

Nardi, F., Vivoni, E. R., and Grimaldi, S.: Investigating a floodplain scaling relation using a hydrogeomorphic delineation method, Water Resources Research, 42, https://doi.org/10.1029/2005WR004155, 2006.

Neumann, B., Vafeidis, A. T., Zimmermann, J., and Nicholls, R. J.: Future Coastal Population Growth and Exposure to Sea-Level Rise and Coastal Flooding - A Global Assessment, PLOS ONE, 10, e0118 571, https://doi.org/10.1371/journal.pone.0118571, 2015.

NOAA: BlueTopo, https://www.fisheries.noaa.gov/inport/item/75311, 2025a.

NOAA: NOAA Atlas 14 Point Precipitation Frequency Estimates: TX, https://hdsc.nws.noaa.gov/pfds/pfds_map_cont.html?bkmrk=tx, 2025b.

Preisser, M., Passalacqua, P., Bixler, R. P., and Hofmann, J.: Intersecting near-real time fluvial and pluvial inundation estimates with sociodemographic vulnerability to quantify a household flood impact index, Hydrology and Earth System Sciences, 26, 3941–3964, https://doi.org/10.5194/hess-26-3941-2022, 2022.

Preisser, M., Passalacqua, P., Bixler, R. P., and Boyles, S.: A network-based analysis of critical resource accessibility during floods, Frontiers in Water, 5, https://www.frontiersin.org/journals/water/articles/10.3389/frwa.2023.1278205, 2023.

Reimann, L., Vafeidis, A. T., and Honsel, L. E.: Population development as a driver of coastal risk: Current trends and future pathways, Cambridge Prisms: Coastal Futures, 1, e14, https://doi.org/10.1017/cft.2023.3, 2023.

Richardson, C. A. and Beighley, R. E.: Optimizing Height Above Nearest Drainage parameters to enable rapid flood mapping in North Carolina, Frontiers in Water, 5, https://doi.org/10.3389/frwa.2023.1296434, 2024.

Samela, C., Troy, T. J., and Manfreda, S.: Geomorphic classifiers for flood-prone areas delineation for data-scarce environments, Advances in Water Resources, 102, 13–28, https://doi.org/10.1016/j.advwatres.2017.01.007, 2017.

Santiago-Collazo, F. L., Bilskie, M. V., and Hagen, S. C.: A comprehensive review of compound inundation models in low-gradient coastal watersheds, Environmental Modelling & Software, 119, 166–181, https://doi.org/10.1016/j.envsoft.2019.06.002, 2019.

Santiago-Collazo, F. L., Bilskie, M. V., Bacopoulos, P., and Hagen, S. C.: Compound Inundation Modeling of a 1-D Idealized Coastal Watershed Using a Reduced-Physics Approach, Water Resources Research, 60, e2023WR035 718, https://doi.org/10.1029/2023WR035718, _eprint: https://onlinelibrary.wiley.com/doi/pdf/10.1029/2023WR035718, 2024.

Schwarz, G. E., Jackson, S. E., and Wieczorek, M. E.: Select Attributes for NHDPlus Version 2.1 Reach Catchments and Modified Network Routed Upstream Watersheds for the Conterminous United States (ver. 4.0, August 2023), https://doi.org/10.5066/F7765D7V, 2018.

Scriven, B. W. G., McGrath, H., and Stefanakis, E.: GIS derived synthetic rating curves and HAND model to support on-the-fly flood mapping, Natural Hazards, 109, 1629–1653, https://doi.org/10.1007/s11069-021-04892-6, 2021.

SETx-UIFL: Southeast Texas Urban Integrated Field Laboratory Annual Report Year 2, https://utexas.app.box.com/s/b9cu8a3qupi8zip32xg2p2xcvi2bvike, 2024.

https://doi.org/10.5194/egusphere-2026-577
Preprint. Discussion started: 20 February 2026

Shen, Y., Morsy, M. M., Huxley, C., Tahvildari, N., and Goodall, J. L.: Flood risk assessment and increased resilience for coastal urban watersheds under the combined impact of storm tide and heavy rainfall, Journal of Hydrology, 579, 124 159, https://doi.org/10.1016/j.jhydrol.2019.124159, 2019.

Shi, P., Lyu, K., Li, Z., Yang, T., Xu, C.-Y., Hao, X., and Xiao, J.: A Novel Topography-Based Approach for Real-Time Flood Inundation Mapping, Water Resources Research, 61, e2024WR037 851, https://doi.org/10.1029/2024WR037851, _eprint: https://onlinelibrary.wiley.com/doi/pdf/10.1029/2024WR037851, 2025.

Silverman, A. I., Brain, T., Branco, B., Challagonda, P. s. v., Choi, P., Fischman, R., Graziano, K., Hénaff, E., Mydlarz, C., Rothman, P., and Toledo-Crow, R.: Making waves: Uses of real-time, hyperlocal flood sensor data for emergency management, resiliency planning, and flood impact mitigation, Water Research, 220, 118 648, https://doi.org/10.1016/j.watres.2022.118648, 2022.

Smith, A. B.: U.S. Billion-dollar Weather and Climate Disasters, https://doi.org/10.25921/STKW-7W73, 2024.

Tellman, B., Sullivan, J. A., Kuhn, C., Kettner, A. J., Doyle, C. S., Brakenridge, G. R., Erickson, T. A., and Slayback, D. A.: Satellite imaging reveals increased proportion of population exposed to floods, Nature, 596, 80–86, https://doi.org/10.1038/s41586-021-03695-w, 2021.

Teng, J., Jakeman, A. J., Vaze, J., Croke, B. F. W., Dutta, D., and Kim, S.: Flood inundation modelling: A review of methods, recent advances and uncertainty analysis, Environmental Modelling and Software, 90, 201–216, https://doi.org/10.1016/j.envsoft.2017.01.006, 2017.

Timilsina, S. and Passalacqua, P.: A comparative analysis of national water model versions 2.1 and 3.0 reveals advances and challenges in streamflow predictions during storm events, Journal of Hydrology: Regional Studies, 58, 102 196, https://doi.org/10.1016/j.ejrh.2025.102196, 2025.

TNRIS: Jefferson, Liberty, & Chambers Counties Lidar, https://data.geographic.texas.gov/collection/?c=12342f12-2d74-44c4-9f00-a5c12ac2659c, 2017.

TxDOT: Hurricane preparation - evacuation and contraflow routes, https://www.txdot.gov/safety/severe-weather/hurricane-preparation.html, 2025.

US Census Bureau: TIGER/Line Shapefiles, https://www.census.gov/geographies/mapping-files/time-series/geo/tiger-line-file.html, section: Government, 2025.

U.S. Congress: JEC Report on Economic Cost of Flooding, https://www.jec.senate.gov/public/index.cfm/democrats/2024/6/flooding-costs-the-u-s-between-179-8-and-496-0-billion-each-year, 2024.

US EPA: NHDPlus Texas Data (Vector Processing Unit 12), https://www.epa.gov/waterdata/nhdplus-texas-data-vector-processing-unit-12, 2015.

USACE: HEC-RAS 2D User's Manual, https://www.hec.usace.army.mil/confluence/rasdocs/r2dum/latest, 2025.

USGS: 3D Elevation Program Digital Elevation Models, https://apps.nationalmap.gov/downloader/#/, 2024.

USGS: Annual National Land Cover Database (NLCD) Collection 1 Products (ver. 1.1, June 2025), https://doi.org/10.5066/P94UXNTS, 2025.

USGS and Arctur, D.: USGS - Harvey High Water Marks, https://doi.org/10.4211/hs.615d426f70cc4346875c725b4b8fdc59, 2018.

van Ormondt, M., Leijnse, T., de Goede, R., Nederhoff, K., and van Dongeren, A.: Subgrid corrections for the linear inertial equations of a compound flood model – a case study using SFINCS 2.1.1 Dollerup release, Geoscientific Model Development, 18, 843–861, https://doi.org/10.5194/gmd-18-843-2025, 2025.

Virtanen, P., Gommers, R., Oliphant, T. E., Haberland, M., Reddy, T., Cournapeau, D., Burovski, E., Peterson, P., Weckesser, W., Bright, J., van der Walt, S. J., Brett, M., Wilson, J., Millman, K. J., Mayorov, N., Nelson, A. R. J., Jones, E., Kern, R., Larson, E., Carey, C. J., Polat, I., Feng, Y., Moore, E. W., VanderPlas, J., Laxalde, D., Perktold, J., Cimrman, R., Henriksen, I., Quintero, E. A., Harris, C. R.,

https://doi.org/10.5194/egusphere-2026-577
Preprint. Discussion started: 20 February 2026

Archibald, A. M., Ribeiro, A. H., Pedregosa, F., van Mulbregt, P., and SciPy 1.0 Contributors: SciPy 1.0: fundamental algorithms for scientific computing in Python, Nature Methods, 17, 261–272, https://doi.org/10.1038/s41592-019-0686-2, 2020.

Wahl, T., Jain, S., Bender, J., Meyers, S. D., and Luther, M. E.: Increasing risk of compound flooding from storm surge and rainfall for major US cities, Nature Climate Change, 5, 1093–1097, https://doi.org/10.1038/nclimate2736, 2015.

Wallemacq, P., Below, R., and McClean, D.: Economic losses, poverty & disasters: 1998-2017, United Nations Office for Disaster Risk Reduction, 2018.

Wang, M., Passalacqua, P., Cai, S., and Dawson, C.: c-HAND: near real-time coastal flood mapping, Frontiers in Water, 6, https://doi.org/10.3389/frwa.2024.1329109, 2024.

Westerink, J. J., Luettich, R. A., Baptists, A. M., Scheffner, N. W., and Farrar, P.: Tide and Storm Surge Predictions Using Finite Element Model, Journal of Hydraulic Engineering, 118, 1373–1390, https://doi.org/10.1061/(ASCE)0733-9429(1992)118:10(1373), 1992.

Zheng, F., Westra, S., and Sisson, S. A.: Quantifying the dependence between extreme rainfall and storm surge in the coastal zone, Journal of Hydrology, 505, 172–187, https://doi.org/10.1016/j.jhydrol.2013.09.054, 2013.

Zheng, X., Maidment, D. R., Tarboton, D. G., Liu, Y. Y., and Passalacqua, P.: GeoFlood: Large-Scale Flood Inundation Mapping Based on High-Resolution Terrain Analysis, Water Resources Research, 54, 10,013–10,033, https://doi.org/10.1029/2018WR023457, 2018.

Zheng, X., D'Angelo, C., Maidment, D. R., and Passalacqua, P.: Application of a Large-Scale Terrain-Analysis-Based Flood Mapping System to Hurricane Harvey, JAWRA Journal of the American Water Resources Association, 58, 149–163, https://doi.org/10.1111/1752-1688.12987, 2022.

Zscheischler, J., Martius, O., Westra, S., Bevacqua, E., Raymond, C., Horton, R. M., van den Hurk, B., AghaKouchak, A., Jézéquel, A., Mahecha, M. D., Maraun, D., Ramos, A. M., Ridder, N. N., Thiery, W., and Vignotto, E.: A typology of compound weather and climate events, Nature Reviews Earth & Environment, 1, 333–347, https://doi.org/10.1038/s43017-020-0060-z, 2020.